

Arresting Ion Migration from the ETL Increases Stability in Infrared Light Detectors Based on III-V Colloidal Quantum Dots

Pan Xia, Tong Zhu, Muhammad Imran, Joao M. Pina, Ozan Atan, Amin Morteza Najarian, Hao Chen, Yangning Zhang, Euidae Jung, Margherita Biondi, Maral Vafaie, Chongwen Li, Luke Grater, Aayushi Khatri, Ajay Singh, Sjoerd Hoogland, and Edward H. Sargent*

III-V colloidal quantum dots (CQDs) are of interest in infrared photodetection, and recent developments in CQDs synthesis and surface engineering have improved performance. Here this work investigates photodetector stability, finding that the diffusion of zinc ions from charge transport layers (CTLs) into the CQDs active layer increases trap density therein, leading to rapid and irreversible performance loss during operation. In an effort to prevent this, this work introduces organic blocking layers between the CQDs and ZnO layers; but these negatively impact device performance. The device is then, allowing to use a C60:BCP as top electron-transport layer (ETL) for good morphology and process compatibility, and selecting NiO_x as the bottom hole-transport layer (HTL). The first round of NiO_x-based devices show efficient light response but suffer from high leakage current and a low open-circuit voltage (Voc) due to pinholes. This work introduces poly[bis(4-phenyl) (2,4,6-trimethylphenyl)amine] (PTAA) with NiO_x NC to form a hybrid HTL, an addition that reduces pinhole formation, interfacial trap density, and bimolecular recombination, enhancing carrier harvesting. The photodetectors achieve 53% external quantum efficiency (EQE) at 970 nm at 1 V applied bias, and they maintain 95% of initial performance after 19 h of continuous illuminated operation. The photodetectors retain over 80% of performance after 80 days of shelf storage.


1. Introduction

Infrared (IR) photodetectors are of interest in automotive and aerospace applications, industrial automation, home appliances, and healthcare applications.^[1–6] Silicon is excellent in the near-IR but then does not extend beyond 1100 nm; while III-V semiconductor materials achieve impressive performance but have limited application due to their high production cost.^[6]

Colloidal quantum dots (CQDs) offer a size-tuned bandgap, solution processing, wavelength tuning, and integration onto a variety of substrates, including read-out integrated circuits.^[1,7,8] In recent years, significant research has focused on the synthesis of III-V CQDs, resulting in progress on increasingly high-performance photodetectors. Recent advancements in synthesis, postsynthesis resurfacing of CQDs, and device engineering have resulted in a rapid rise to 37% external quantum efficiency (EQE) at 1 V bias.^[9–14] There remains room, though, to devices' operating stability,

P. Xia, T. Zhu, M. Imran, J. M. Pina, O. Atan, A. M. Najarian, H. Chen, Y. Zhang, E. Jung, M. Biondi, M. Vafaie, C. Li, L. Grater, S. Hoogland, E. H. Sargent
Department of Electrical and Computer Engineering
University of Toronto
10 King's College Road, Toronto, Ontario M5S 3G4, Canada
E-mail: ted.sargent@utoronto.ca

A. Khatri, A. Singh
STMicroelectronics
Digital Front-end Manufacturing & Technology
Technology for Optical Sensors
Fremont, California 94538, USA

 The ORCID identification number(s) for the author(s) of this article can be found under <https://doi.org/10.1002/adma.202310122>

© 2023 The Authors. Advanced Materials published by Wiley-VCH GmbH. This is an open access article under the terms of the Creative Commons Attribution-NonCommercial-NoDerivs License, which permits use and distribution in any medium, provided the original work is properly cited, the use is non-commercial and no modifications or adaptations are made.

DOI: 10.1002/adma.202310122

Table 1. Comparison of operating and shelf stability of colloidal quantum dots (CQDs) based infrared (IR)-photodetectors.

Types	Materials	Detectivity (D^*) [Jones]	Frequency (f) [Hz]	Performance loss upon storage	Performance loss under operation
Phototransistor	PbS ^[17,24]	3.4×10^8	40	60 days	--
	PbS/IGZO ^[25]	1.1×10^{13}	–	10% after 120 days	--
Photoconductor	HgTe ^[26]	2.0×10^7	–	–	--
	Perovskite/PbS ^[27]	2.6×10^{12}	5.8×10^3	10% after 150 days	--
Photodiode	PbS ^[28]	8.0×10^{11}	–	–	25% after 12 h
	PbS ^[2]	2.1×10^{12}	1.4×10^5	0% after 30 days	–
	PbS/Perovskite ^[29]	6.2×10^{12}	–	–	5% after 0.5 h
This work	InAs-conventional	1.9×10^{11}	6.5×10^6	50% after 6 days	50% after 1.5 h
	InAs-hybrid HTLs	6.9×10^{11}	6.5×10^6	14% after 90 days	5% after 19 h

also an important metric when evaluating photodetectors **Table 1**.

We assessed degradation in InAs CQD-based devices and found evidence of zinc leaching from the ZnO electron-transport layer (ETL). When we sought to use organic blocking layers to prevent this degradation, we were not able to do so without negatively impacting performance. Turning to charge transport layer engineering, we found that NiO_x provided both high stability and also high optical transparency beneficial; but that it led to high leakage currents, a finding we linked to pinholes in CQD films. Inserting a poly[bis(4-phenyl) (2,4,6-trimethylphenyl)amine (PTAA) interlayer overcame these problems, and these enabled us to report a 53% EQE at 960 nm. The resultant devices retain 95% of their initial performance over the course of 19 h of operation. The devices also retained 80% performance following 80 days of shelf storage.

2. Results and Discussion

In order to assess the operating stability of devices, we fabricated photodetectors based on InAs CQDs using established methods (ITO/ZnO-NP/InAs-CQDs/MoOx/Ag, denoted as conventional photodetector)^[10,15] (Figure S1, Supporting Information). These devices showed 40% external quantum efficiency (EQE) at 970 nm, a dark current of 4×10^{-4} mA cm⁻² at a reverse bias of 1 V, and a rectification ratio of 10^6 (Figure 1a,b). These results are on par with recent InAs CQDs photodetector reports.^[15]

To evaluate operating stability, we investigated transient photocurrent (TPC) response under pulsed laser illumination, without applying bias. The TPC showed a 90% loss in response following 8 h of illuminated operation (Figure 1c). The open-circuit voltage (Voc) also decreased rapidly under uninterrupted illumination (Figures S1 and S2, Supporting Information). Both observations suggest the dissipation of the built-in electrical field over time.

We used solar cell capacitance simulator (SCAPS) with a previous reported model to study how trap density and n-doping impact performance (Figure S3, Supporting Information)^[16] From device cross-sections (Figure 1f) using scanning transmission electron microscopy (STEM) coupled with energy-dispersive X-ray spectroscopy, we found that zinc had traveled from the ETL

into the CQDs layer, with a 3% atomic abundance at a depth of 100 nm inside the active layer (Figure 1e and Figure S4, Supporting Information).

We used density functional theory simulation to look at how zinc may affect the electronic structure of InAs CQDs. We first built the InAs CQDs models passivated with bromide (Br, passivating the surface In atoms) and indium bromide (InBr₂, passivating the surface As atoms) species as reported previously (Figure 1g).^[16] We introduced Zn at different positions (interstitial, antisite central, and antisite surface) in InAs CQDs. Zn in the interstitial position generates additional deep energy levels within the bandgap. This is in agreement with previous studies which show that interstitial substitution of In with Zn in InP CQDs produces in-gap-states.^[17,18] Conversely, the gap remained unaltered when Zn was incorporated at the antisite central and antisite surface sites.

In an effort to impede ion migration from the ZnO into the active layer, we introduced polymer-based blocking layers, polymer-PDIN (N,N'-Bis[3-(dimethylamino) propyl]perylene-3,4,9,10-tetracarboxylic diimide), and also phenyl-C61-butyric acid methyl ester (PCBM) between the active layer and ZnO ETL; however, each of these led to loss in device performance (Figure S5, Supporting Information), as did our attempts to change the ETL to SnO₂ (Figure S6, Supporting Information). Among candidate causes of the loss of performance, we propose: (1) the materials processing of the CQD layer, which may compromise the integrity of the blocking layer; (2) the modest charge carrier mobilities in such layers.

We considered applying the device structure to replace the current charge transport layers (CTLs) with Zn-free materials. For the bottom hole-transport layer (HTL), we focused on NiO_x for its high charge carrier mobility, stable composition, and high optical transparency in the near-IR range (Figure 2a). Specifically, we employed NiO_x NCs annealed at 270 °C.^[19–21] For the ETL, C60:BCP is chosen due to its good electron mobility and thermal stability.^[19] However, the wettability of InAs QD on C60 film is poor (Figure S7, Supporting Information). Therefore, we inverted the device structure from n-i-p (NIP) to p-i-n (PIN), allowing using C60:BCP on the top of CQD. The current density characteristics of photodetectors are reported in Figure 2b. The current density characteristics of photodetectors are reported in Figure 2b.

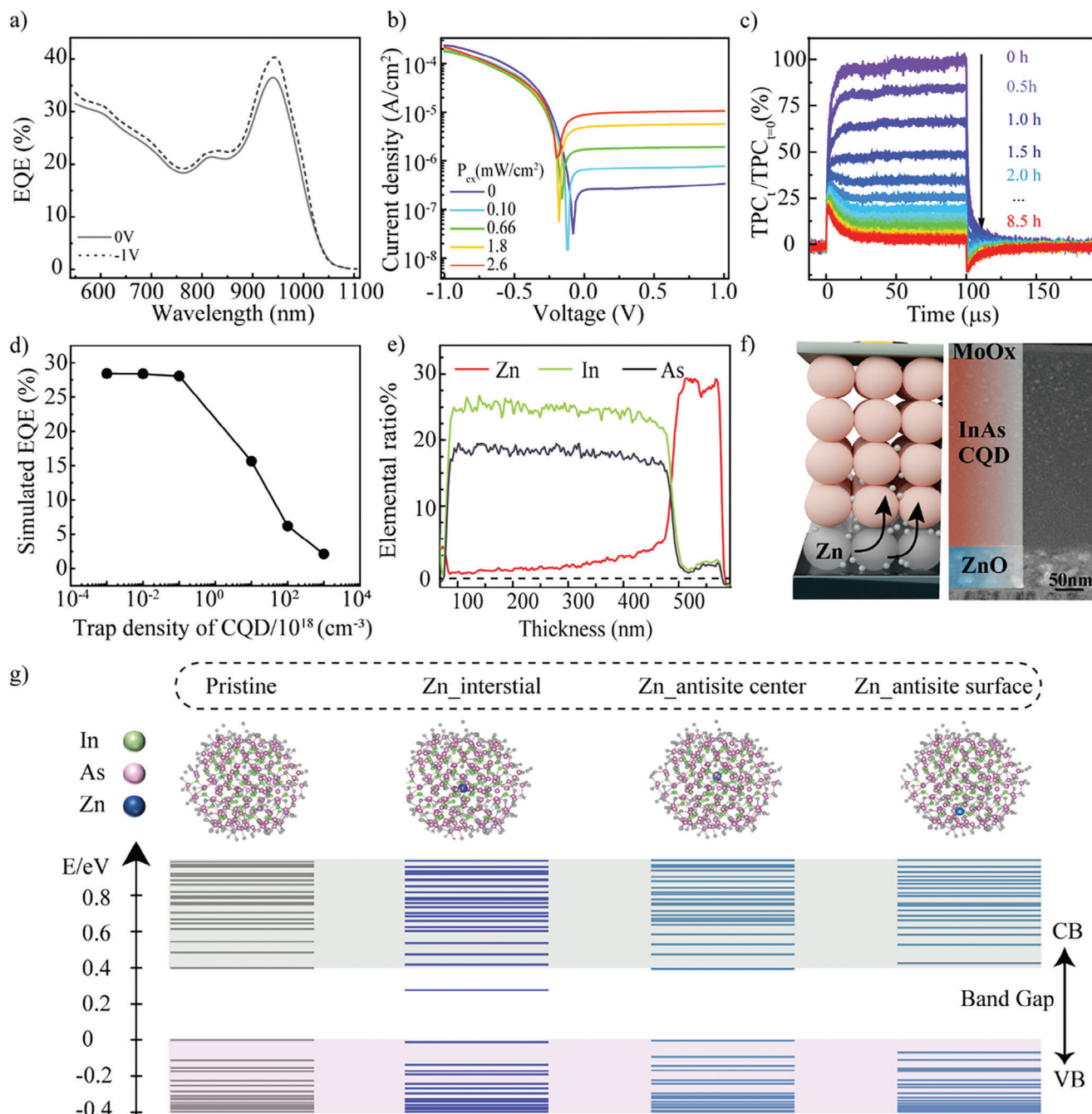


Figure 1. Investigations of causes of performance losses in InAs photodetectors: a) External quantum efficiency (EQE) of InAs quantum-dot-based photodetectors in the conventional NIP (n-i-p) structure; device stack in Figure 1f. b) Current–voltage characteristics at various illumination powers; and c) transient photocurrent (TPC) stability under 850 nm laser light irradiation. d) Simulated EQE of InAs colloidal quantum dots (CQDs) photodetectors from SCAPS simulation with different InAs CQDs trap densities. e) Elemental distribution (In, As, and Zn) across the photodetector. f) Scanning transmission electron microscopy (STEM) image of photodetector cross-section and schematic of the device structure. g) Electronic structures (top) and the associated calculated energy diagrams for the passivated InAs CQDs (gray) and those with one Zn ion in different positions within the InAs CQDs.

These devices exhibited good light response and thermal stability (as evidenced by time-of-flight secondary ion mass spectrometry (ToF-SIMS) analysis reported in Figure S7a, Supporting Information); but they suffered from high leakage current and low Voc. Atomic force microscopy (AFM) analysis of CQDs

films on HTL revealed both high surface roughness and the presence of pinholes in the film. These factors contribute to electrical shunting, leading to current leakage and a reduction in Voc.

Pinholes have previously been seen in NiO_x NC layers and InAs CQDs (Figure 2e),^[22,23] increasing leakage current.

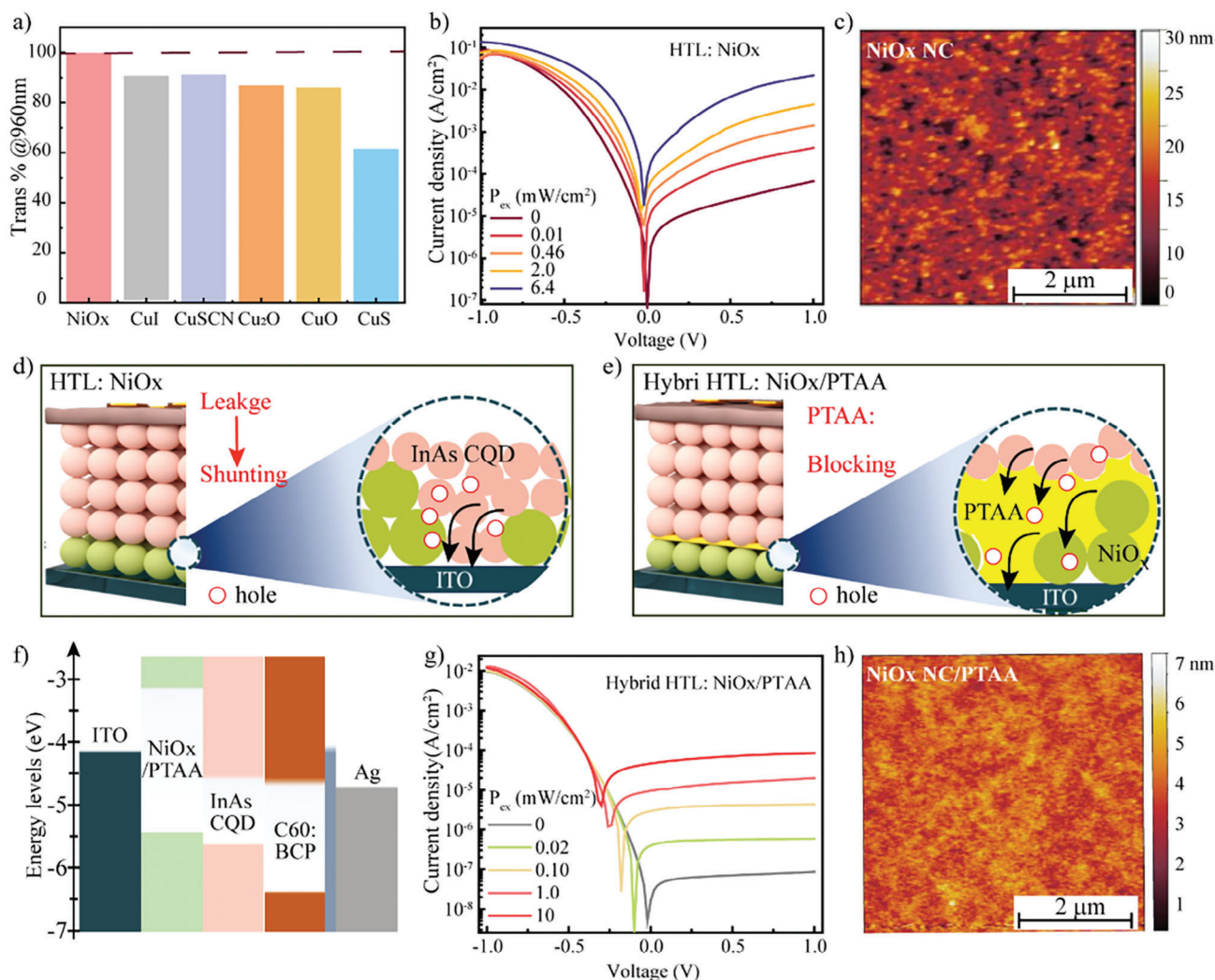


Figure 2. Engineering charge transport layers in InAs colloidal quantum dots (CQDs) photodetectors. a) Transmittance of different metal oxide hole-transport layers (HTLs) at 970 nm (see details in Figure S8, Supporting Information). b) Current–voltage characteristics of the photodetector with NiO_x NC as HTL at various illumination powers. c) Atomic force microscopy (AFM) analysis of the NiO_x NC film. d,e) The PIN (p-i-n) architecture photodetector with and without poly[bis(4-phenyl) (2,4,6-trimethylphenyl)amine (PTAA) as the modifier revealing the electrical shunting caused by pinholes in the NiO_x film (d) and their filling and smoothing by the PTAA modifier (e). f) The energy diagram of the hybrid-HTLs-based PIN photodetectors. g) The behavior of current density versus voltage under varying illumination for an improved photodetector with hybrid HTLs. h) AFM of hybrid NiO_x and PTAA film.

After scanning the suitable band-alignment polymers including poly(3,4-ethylenedioxythiophene) polystyrene sulfonate (PEDOT:PSS) and PTAA (Figure S8, Supporting Information), we chose PTAA as an interlayer achieving a threefold reduction in dark current and improved V_{oc} of 0.4 V. We measured the optical transmittance of PTAA on NiO_x film and found this to be unchanged in the infrared spectral range (Figure S8b, Supporting Information). GISASX indicates better dot ordering on the hybrid HTLs in comparison to conventional ZnO-based film (see Figure S9, Supporting Information).

AFM analysis indicates improved film roughness and reduced pinholes when PTAA layer is added (Figure 2h). The valence band (VB) of NiO_x NC shifted upwards by 0.2 eV, facilitating hole extraction from the InAs CQDs layer (Figure S10, Supporting Information). Power-dependent V_{oc} and short-circuit current (J_{sc})

revealed a reduced bimolecular recombination rate (Figure S11, Supporting Information). Pump-probe transient absorption (TA) spectroscopy revealed that in NiO_x/PTAA CQDs films, the exciton peak returned to its ground state faster than in NiO_x films alone, potentially due to fewer interfacial defects and improved band alignment (Figure S12, Supporting Information). SCAPS device modeling agreed with these findings, suggesting a better band alignment in NiO_x/PTAA and fewer interface traps (Figure S13, Supporting Information).

We then examined the compositional stability of charge transport layers in the optimized photodetector stack using ToF-SIMS. We saw no measurable evidence of ion migration into the active layer following 80 days of storage (Figure 3a and Figure S14, Supporting Information). Composition was also stable after subjecting the films to annealing at 120 °C for 10 h.

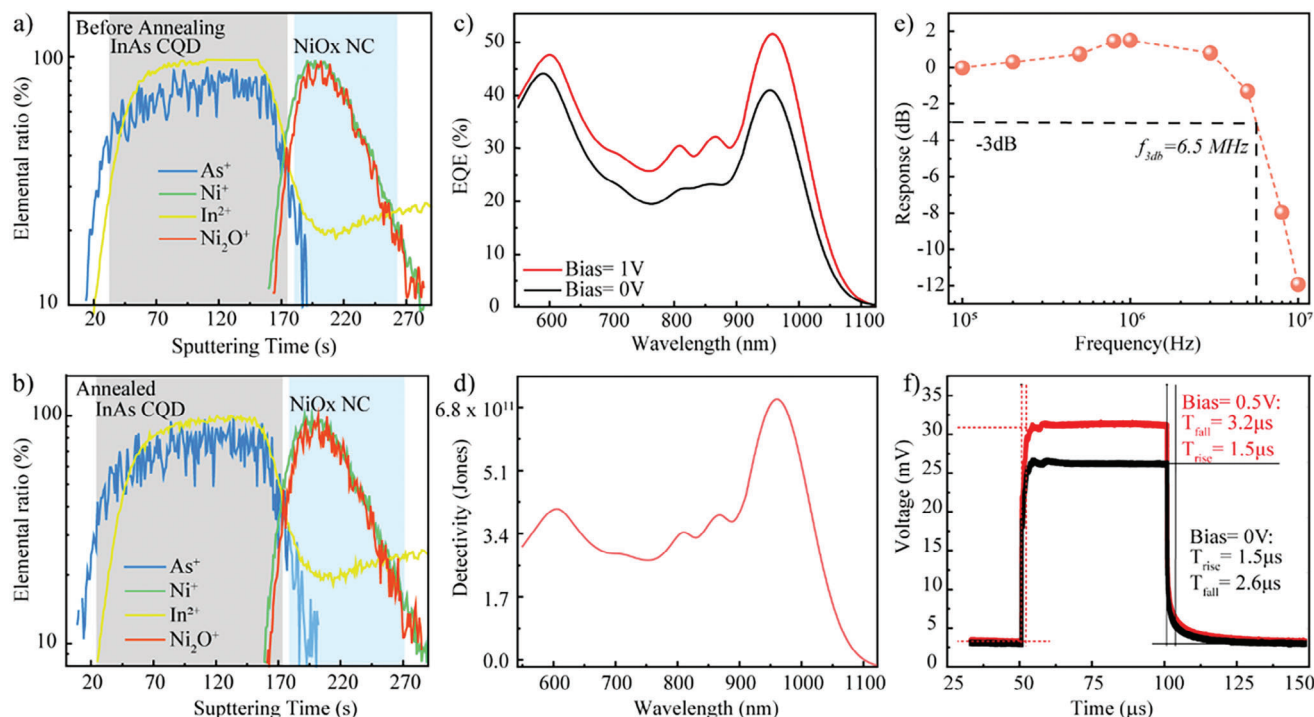


Figure 3. Optimization of hybrid hole-transport layer (HTL) based photodetectors: a,b) Time-of-flight secondary ion mass spectrometry (ToF-SIMS) ion depth profile obtained from a p-i-n (PIN) photodetector with and without heating at 120 °C for 10 h. The NiO_x NC layer and the colloidal quantum dots (CQDs) layer are indicated on the profile. c) External quantum efficiency (EQE) of the PIN photodetector devices; d) Detectivity, calculated with noise at 10 kHz using a signal analyzer. e) Normalized signal response as a function of the light modulation frequency, showing that the f_{3dB} bandwidth of the device is 6.5 MHz. The pixel size is 0.03 mm², and the response is measured without bias. f) The transient photocurrent (TPC) of 0.049 cm² photodetectors.

Frequency-dependent capacitance measurements of devices showed minor variation for NiO_x/PTAA compared to ZnO-based photodetectors (Figure S15, Supporting Information).

We further optimized the active layer thickness in the detectors, reaching an EQE of 53% with a thickness of 150 nm (Figure S16, Supporting Information) and Figure 3c,d shows responsivity and detectivity, with values of 0.4 A W⁻¹ and 6.9 × 10¹¹ Jones (threefold higher than the conventional NIP devices) at 970 nm photoexcitation wavelength. The 3-dB bandwidth (f_{3dB}) was 6.5 MHz (Figure 3e).

We studied operating stability under 850 nm laser light in a nitrogen environment (Figure 4c). Conventional devices fabricated using NIP architectures lost 95% (retained 5%) of the initial photocurrent after 8 h. In contrast, hybrid-HTL-based devices retained 95% of the initial photocurrent following 19 h of continuous, unbiased operation. This is, to the best of our knowledge, the highest operating and shelf stability reported among infrared III-V CQD-based devices (Figure 4e).

3. Conclusion

In summary, we examined the instability issues in conventional CQDs-based photodetectors and identified ion migration from a Zn-containing ETL into the active layer as one leading cause of degradation. We inverted the devices and added a hybrid hole transport layer consisting of NiO_x and PTAA. Devices reached 53% EQE at 970 nm and a detectivity of 6 × 10¹¹ Jones as well

as improved operating stability, retaining 95% of initial performance after 20 h of continuous illuminated operation. The high surface-to-volume ratio of CQDs makes them susceptible to external factors such as ion migration and oxidation.^[30,31] The results of this study underscore the critical role, in device stability, of a unified emphasis on transport layers and the CQD active layer.

4. Experimental Section

See Supporting Information.

Supporting Information

Supporting Information is available from the Wiley Online Library or from the author.

Acknowledgements

P.X., T.Z., and M.I. contributed equally to this work. The authors thank Larissa Levina and Elenita Palmiano for the synthesis and washing of CQDs. Authors also thank Remi Wolowiec and Damir Kopilovic for their assistance throughout the study. Part of the research described in this paper was performed at the Canadian Light Source, a national research facility of the University of Saskatchewan, which is supported by the Canada Foundation for Innovation (CFI), the Natural Sciences and Engineering Research Council (NSERC), the National Research Council (NRC), the Canadian Institutes of Health Research (CIHR), the Government of Saskatchewan,

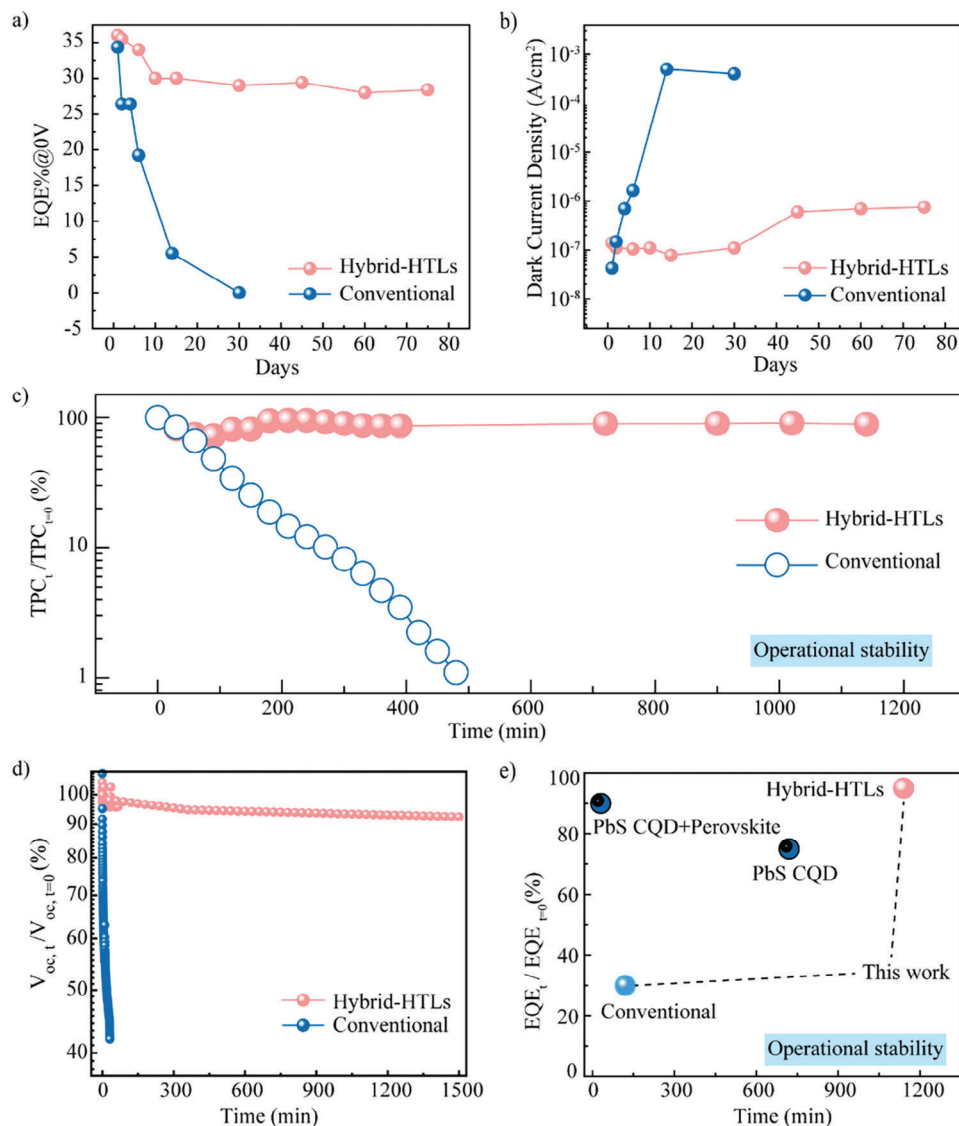


Figure 4. Operating and shelf stability of conventional versus hybrid hole-transport layer (HTL) based photodetectors. a,b) External quantum efficiency (EQE) and dark current of photodetectors upon aging. The devices were stored in a nitrogen-filled glovebox. c) Transient photocurrent (TPC) stability test of conventional and hybrid-HTL-based InAs colloidal quantum dots (CQDs) based photodetectors for continuous 19 h of operation under 850 nm laser excitation ($J-V$ before and after TPC measurement is shown in Figures S17 and S18, Supporting Information). d) Open-circuit voltage (V_{oc}) stability of conventional and hybrid-HTLs photodetectors under 850 nm light. e) Comparison of operational stability of CQDs-based infrared (IR) photodetectors reported here versus prior studies (Table 1). TPC measurements are conducted without bias.

and the University of Saskatchewan. ToF-SIMS was performed at the University of Toronto's Open Centre for the Characterization of Advanced Materials (OCCAM). The authors gratefully acknowledge funding from STMicroelectronics.

Conflict of Interest

The authors declare no conflict of interest.

Data Availability Statement

The data that support the findings of this study are available from the corresponding author upon reasonable request.

Keywords

III-V colloidal quantum dots, charge transport layers, device operating stability, infrared photodetectors

Received: September 30, 2023

Revised: November 9, 2023

Published online:

- [1] J. S. Steckel, E. Josse, A. G. Pattantyus-Abraham, M. Bidaud, B. Mortini, H. Bilgen, O. Arnaud, S. Allegret-Maret, F. Saguin, L. Mazet, S. Lhostis, T. Berger, K. Haxaire, L. L. Chapelon, L. Parmigiani, P.

- Gouraud, M. Brihoum, P. Bar, M. Guillermet, S. Favreau, R. Duru, J. Fantuz, S. Ricq, D. Ney, I. Hammad, D. Roy, A. Arnaud, B. Vianne, G. Nayak, N. Virollet, et al., in *2021 IEEE International Electron Devices Meeting*, IEEE, Piscataway, NJ **2021**, p. 23.4.1.
- [2] J. Liu, P. Liu, D. Chen, T. Shi, X. Qu, L. Chen, T. Wu, J. Ke, K. Xiong, M. Li, H. Song, W. Wei, J. Cao, J. Zhang, L. Gao, J. Tang, *Nat. Electron.* **2022**, *5*, 443.
- [3] F. Xu, X. Liu, K. Fujimura, *IEEE Transactions on Intelligent Transportation Systems*, Vol. 6, IEEE, Piscataway, NJ **2005**, p. 63.
- [4] A. M. Gorbach, J. D. Heiss, L. Kopylev, E. H. Oldfield, *J. Neurosurg.* **2004**, *101*, 960.
- [5] M. S. Jadin, S. Taib, *Infrared Phys. Technol.* **2012**, *55*, 236.
- [6] C. L. Tan, H. Mohseni, *Nanophotonics* **2018**, *7*, 169.
- [7] E. Georgitzikis, P. Malinowski, Y. Li, J. Lee, A. Suess, F. Frazzica, J. Maes, S. Gielen, F. Verstraeten, P. Boulenc, M. Mao, S. Guerrieri, W. Maes, H. Zeger, P. Heremans, D. Cheyns, In Proceedings of the 2019 International Image Sensor Workshop (IISW), Snowbird, Utah, USA, **2019**.
- [8] M. Biondi, M.-J. Choi, Z. Wang, M. Wei, S. Lee, H. Choubisa, L. K. Sagar, B. Sun, S.-W. Baek, B. Chen, P. Todorović, A. M. Najarian, A. Sedighian Rasouli, D.-H. Nam, M. Vafaie, Y. C. Li, K. Bertens, S. Hoogland, O. Voznyy, F. P. García de Arquer, E. H. Sargent, *Adv. Mater.* **2021**, *33*, 2101056.
- [9] J. Leemans, V. Pejović, E. Georgitzikis, M. Minjauw, A. B. Siddik, Y.-H. Deng, Y. Kuang, G. Roelkens, C. Detavernier, I. Lieberman, P. E. Malinowski, D. Cheyns, Z. Hens, *Adv. Sci.* **2022**, *9*, 2200844.
- [10] B. Sun, A. M. Najarian, L. K. Sagar, M. Biondi, M.-J. Choi, X. Li, L. Levina, S.-W. Baek, C. Zheng, S. Lee, A. R. Kirmani, R. Sabatini, J. Abed, M. Liu, M. Vafaie, P. Li, L. J. Richter, O. Voznyy, M. Chekini, Z.-H. Lu, F. P. García de Arquer, E. H. Sargent, *Adv. Mater.* **2022**, *34*, 2203039.
- [11] M.-J. Choi, L. K. Sagar, B. Sun, M. Biondi, S. Lee, A. M. Najjariyan, L. Levina, F. P. García de Arquer, E. H. Sargent, *Nano Lett.* **2021**, *21*, 6057.
- [12] J. H. Song, H. Choi, H. T. Pham, S. Jeong, *Nat. Commun.* **2018**, *9*, 4267.
- [13] P. Xia, B. Sun, M. Biondi, J. Xu, O. Atan, M. Imran, H. Yasser, Y. Liu, J. Pina, A. Najarian, L. Grater, K. Bertens, L. K. Sagar, H. Anwar, M.-J. Choi, Y. Zhang, M. Hasham, F. P. G. de Arquer, S. Hoogland, M. W. B. Wilson, E. H. Sargent, *Adv. Mater.* **2023**, *35*, 2301842.
- [14] M. Imran, D. Choi, D. H. Parmar, B. Rehl, Y. Zhang, O. Atan, G. Kim, P. Xia, J. M. Pina, M. Li, Y. Liu, O. Voznyy, S. Hoogland, E. H. Sargent, *Adv. Mater.* **2023**, *35*, 2306147.
- [15] P. Xia, B. Sun, M. Biondi, J. Xu, O. Atan, M. Imran, Y. Hassan, Y. Liu, J. M. Pina, A. M. Najarian, L. Grater, K. Bertens, L. K. Sagar, H. Anwar, M.-J. Choi, Y. Zhang, M. Hasham, F. P. G. de Arquer, S. Hoogland, M. W. B. Wilson, E. H. Sargent, *Adv. Mater.* **2023**, *35*, 2301842.
- [16] T.-G. Kim, D. Zherebetskyy, Y. Bekenstein, M. H. Oh, L.-W. Wang, E. Jang, A. P. Alivisatos, *ACS Nano* **2018**, *12*, 11529.
- [17] H. Cho, S. Jung, M. Kim, H. Kwon, J. Bang, *J. Lumin.* **2022**, *245*, 118647.
- [18] E. M. Janke, N. E. Williams, C. She, D. Zherebetskyy, M. H. Hudson, L. Wang, D. J. Gosztola, R. D. Schaller, B. Lee, C. Sun, G. S. Engel, D. V. Talapin, *J. Am. Chem. Soc.* **2018**, *140*, 15791.
- [19] H. Chen, S. Teale, B. Chen, Y. Hou, L. Grater, T. Zhu, K. Bertens, S. M. Park, H. R. Atapattu, Y. Gao, M. Wei, A. K. Johnston, Q. Zhou, K. Xu, D. Yu, C. Han, T. Cui, E. H. Jung, C. Zhou, W. Zhou, A. H. Proppe, S. Hoogland, F. Laquai, T. Filleter, K. R. Graham, Z. Ning, E. H. Sargent, *Nat. Photonics* **2022**, *16*, 352.
- [20] H. Chen, Z. Peng, K. Xu, Q. Wei, D. Yu, C. Han, H. Li, Z. Ning, *Sci China Mater.* **2021**, *64*, 10.
- [21] F. Jiang, W. C. H. Choy, X. Li, D. Zhang, J. Cheng, *Adv. Mater.* **2015**, *27*, 2930.
- [22] Y. Wang, L. Duan, M. Zhang, Z. Hameiri, X. Liu, Y. Bai, X. Hao, *Sol. RRL* **2022**, *6*, 2200234.
- [23] M. Stolterfoht, C. M. Wolff, J. A. Márquez, S. Zhang, C. J. Hages, D. Rothhardt, S. Albrecht, P. L. Burn, P. Meredith, T. Unold, D. Neher, *Nat. Energy* **2018**, *3*, 847.
- [24] C. Hu, A. Gassenq, Y. Justo, K. Devloo-Casier, H. Chen, C. Detavernier, Z. Hens, G. Roelkens, *Appl. Phys. Lett.* **2014**, *105*, 171110.
- [25] Y.-S. Kim, H.-J. Oh, S. Shin, N. Oh, J.-S. Park, *Sci. Rep.* **2022**, *12*, 12167.
- [26] X. Tang, X. Tang, K. W. C. Lai, *ACS Photonics* **2016**, *3*, 2396.
- [27] W. Pan, M. Tan, Y. He, H. Wei, B. Yang, *Nano Lett.* **2022**, *22*, 2277.
- [28] M. Vafaie, J. Z. Fan, A. Morteza Najarian, O. Ouellette, L. K. Sagar, K. Bertens, B. Sun, F. P. García de Arquer, E. H. Sargent, *Matter* **2021**, *4*, 1042.
- [29] D. Chen, Y. Liu, B. Xia, L. Chen, Y. Yang, G. Yang, J. Liu, S. Lu, C. Ge, P. Liu, J. Yang, G. Liang, X. Lan, X. Zeng, L. Li, J. Zhang, Z. Xiao, L. Gao, J. Tang, *Adv. Funct. Mater.* **2023**, *33*, 2210158.
- [30] Y. Zhang, M. Vafaie, J. Xu, J. M. Pina, P. Xia, A. M. Najarian, O. Atan, M. Imran, K. Xie, S. Hoogland, E. H. Sargent, *Adv. Mater.* **2022**, *34*, 2206884.
- [31] L. Chen, J. Liu, P. Liu, S. Lu, Y. Yang, X. Liang, L. Zhang, J. Hu, J. Yang, Y. Liu, W. Ma, X. Zhao, X. Lan, J. Zhang, L. Gao, J. Tang, *ACS Photonics* **2023**, *10*, 2374.